Dynamical behavior of 100-Å x-ray emissions from picosecond-laser plasmas in various target materials

Noboru Nakano* and Hiroto Kuroda
The Institute for Solid State Physics, The University of Tokyo, Minato-ku, Tokyo 106, Japan
(Received 28 October 1985; revised manuscript received 16 December 1986)

The dynamical behavior of x-ray emissions ranging from 90 to 110 Å generated from laser plasmas is studied and x-ray energies are measured for various target materials with the atomic number from 13 to 82. With the use of a picosecond YAG laser (YAG represents yttrium aluminum garnet), characteristic decay times can be obtained accurately and varied from 100 to 800 ps as functions of target materials. It is also found that the decay times are well correlated with x-ray energies as functions of the atomic number. From this correlation, the atomic-number dependence of decay times can be explained by considering that line x rays are emitted mainly through the radiative recombination processes. X-ray decay times can be measured correctly using a picosecond laser. The dynamical behavior of x-ray energies is explained by the computational result performed for aluminum as an example in the framework of a transient collisional radiative model.

I. INTRODUCTION

For laser fusion research, the measurement of x-rays from laser plasmas is widely used as a diagnostic tool for evaluation of electron temperatures and densities.[1–13] Many works concerning characteristics of x rays are presented along this line. Recently x-ray lasers have attracted keen interest and an x-ray amplification experiment was reported using laser plasmas.[14] Population densities are changed within a picosecond time scale and dynamic processes related to plasma parameters affect conditions of population inversions. X-rays from laser plasmas are useful also for microfabrication and absorption spectroscopy.[15,16] From these viewpoints, it is important to investigate the dynamic behavior of x-ray emissions for many purposes. Wavelength bands near 100 Å have attracted keen interest especially for x-ray laser study.[14,17] But few studies have been reported concerning the dynamic behavior of x-ray emissions near 100 Å from laser plasmas. Most works using high-power lasers have been mainly concerned with laser fusion projects and many experiments have been performed by subnanosecond or nanosecond lasers[18–22] and picosecond lasers[23–26] in the x-ray band below 10 Å.

This paper presents various results and discussions clarifying the dynamic behavior of x-ray emissions near 100 Å from laser-produced plasmas using various targets. We found that x-ray emission decay times vary from 100 to 800 ps depending on the target materials. X-ray energies are also measured as functions of the atomic number of target materials. The dependence of x-ray energies on the atomic number correlates well with x-ray decay. From this correlation, the atomic-number dependence of decay times can be explained by considering that line x rays emit mainly through radiative recombination processes. X-ray decay times can be measured correctly using a picosecond laser. We describe experiments in Sec. II and discussions in Sec. III.

II. EXPERIMENTS AND RESULTS

Figure 1 shows a schematic diagram of our experiments. A single pulse is emitted from a YAG mode-locked oscillator (where YAG represents yttrium aluminum garnet) and amplified by four stage amplifiers to 100 mJ for 30 ps of pulse width. This pulse is focused by a lens of 150-mm focal length on a target set in a vacuum chamber. Spectra ranging from 10 to 300 Å were obtained by a newly developed flat-field spectrometer.[27] The spectrometer has the advantage of offering flat spectra on the focal plane using a grating with rulings of varied pitches. Therefore, a coupling with two-dimensional flat detectors, such as a streak camera, a microchannel plate (MCP), photographic film, and a diode array can be easily performed. Vacuum chamber, spectrometer, and streak camera were evacuated to 2×10^{-6} Torr to avoid damage from a high-voltage breakdown. For this experiment, a grating with 1200 grooves/mm average pitch was used with an incidence angle of 87°. Part of the spectral range centered at 100 Å with a bandwidth of about 10 Å [full width at half maximum (FWHM)] was selected and time-resolved by a streak camera. We are interested in this spectral band, because it is important for x-ray laser study. For instance, x-ray amplification was reported at about 200 Å (Ref. 14) and a proposal for short-wavelength

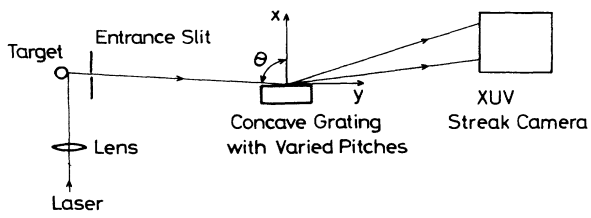

FIG. 1. An experimental setup. A streak camera is set at the focal position of a newly developed flat-field spectrometer.

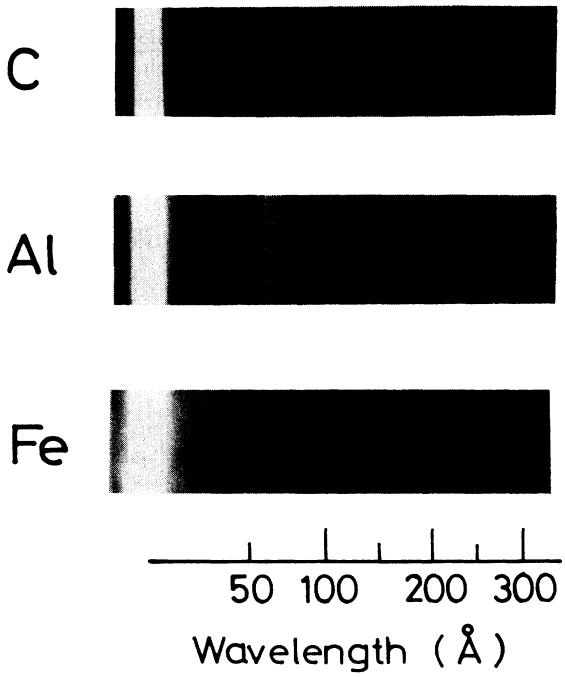

FIG. 2. A typical spectrograph.

lasing was also reported.[17] Time-resolved streaked images, taken by an intensified silicon-intensifier camera, were stored in the frame memory. The wavelength average of these images in the band 100±10 Å was performed by a microcomputer.

Typical spectra are shown in Fig. 2. In this spectral range, line x-ray energies are stronger than continuum x-ray energies. The temporal behavior of observed x-ray energies in the band 100±10 Å is mainly due to line x-ray energies. In this paper average values of x-ray decays are treated in the wavelength band 100±10 Å, but, in this band, x-ray lines with especially shorter or longer decays than these average values cannot be observed. Figure 3

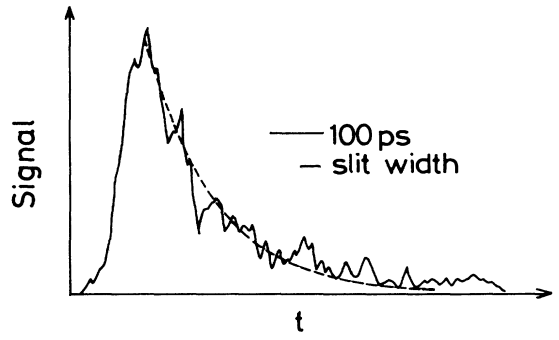

FIG. 3. A typical result of temporal change of x-ray energies emitted from laser plasmas for Zr target. A time resolution of about 40 ps is determined by a slitwidth and a scan speed used in these experiments.

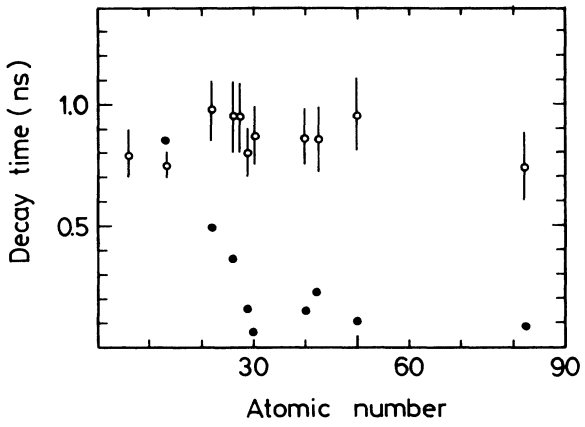

FIG. 4. Closed circles show decay times as functions of the atomic number. Open circles indicate the time when the ion collector picks up signals (×1/1000).

shows a typical result of a temporal change of the x-ray energies from laser plasmas from Zr targets. As shown in this figure, x-ray energies decay slowly compared to the 30-ps laser pulse width. This curve can be fitted well with a single exponential decay curve expressed as a dotted line in that figure and a decay time is easily obtained.

Figure 4 summarizes decay times of line x rays for various targets as functions of atomic number. Decay times decrease with increasing atomic number—for instance, 800 ps for aluminum and 100 ps for copper. As discussed in Sec. III, decays of electron densities and temperatures affect x-ray decays. To estimate the effect, it should be made clear that velocities strongly depend on atomic numbers. In Fig. 4, the time t when the ion collector picks up signals is also shown as an open circle. This collector is set at 10 cm (l) from the target. Plasma front velocities which are defined as l/t show little change as a function of atomic number compared with decay times of x-ray energies.

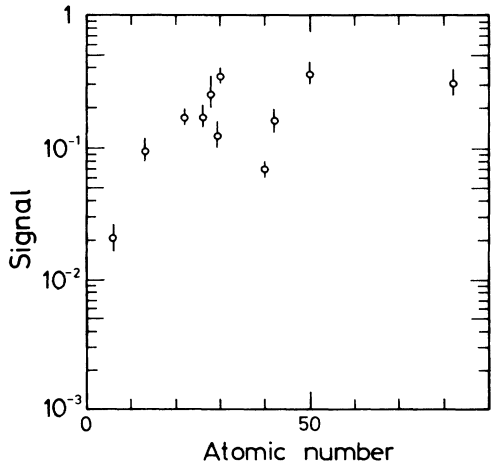

FIG. 5. X-ray energies as functions of the atomic number.

TABLE I. Transitions in the region at about 100 Å.

Z	Target	Charge state	Transition	Ref.
13	Al	4	$2p$-$3d$, $2p$-$4s$	26,27
		5	$3s$-$2p$	
22	Ti	9,11	$3s$-$5p$, $3s$-$4p$, $3p$-$5d$, $3p$-$4d$, $3p$-$4s$, $3d$-$4f$, $3d$-$5f$, $3d$-$6f$	28–30
26	Fe	17,20	$2s$-$2p$	31–33
29	Cu	7,8	$3d$-$4f$	34
		20	$4f$-$5g$	35,36
30	Zn	8	$3d$-$4f$	34
		19	$4d$-$5p$, $4d$-$5f$, $4f$-$5g$	35,36,37
40	Zr	11	$4s$-$5p$, $4p$-$5d$	38
		13	$3p$-$3d$	39
42	Mo	13	$4p$-$5d$, $4d$-$5f$, $4p$-$5s$	38
50	Sn	20	$4s$-$5p$ (40–80 Å)	27
		20,21	$4s$-$4p$ ($\sim$200Å)	40

Next, x-ray energies in the band 100±10 Å are measured using a combination of plastic scintillator and a photo multiplier. Figure 5 shows results as functions of atomic number. As shown, x-ray energies vary extremely starting at about atomic number 30.

III. DISCUSSION

Decay times and energies of x rays at about 100 Å from laser plasmas have been measured as functions of atomic number using a picosecond laser. Here we discuss the origins of measured emissions and consider several reasons for the origin of the atomic-number dependence of x-ray decay times.

A. Origins of measured emissions

Possible emission lines in the 100±10-Å band appearing in Refs. 28–42 are listed in Table I. Wavelengths of Sn lines are slightly outside the 100±10-Å band, but these lines are listed in the table as a reference. In our limited knowledge, lines of Pb are not well known. In this spectral band, the longest radiative lifetimes of these lines are about 20 ps. Measured decay times from about 100 to 800 ps are determined by the quenching of the process that upper states concerning emissions are excited through the recombination processes.[12,19] To confirm this explanation computations using a transient collisional radiative (CR) model were performed for aluminum plasmas (see the Appendix). Experimental results can be explained successfully by computational ones with adjusting laser energies. The effect of a decrease of temperatures, densities, and populations on x-ray decays through recombination processes can also be evaluated. From computational results, it is clear that radiative recombination plays a dominant role after 100 ps. X-ray decay times from 100 to 800 ps can be measured correctly using a picosecond laser.

B. Atomic-number dependence of decay times of x rays

We present here the equation for x-ray energies and show quantitatively how dynamic processes which have picosecond-order characteristic times influence temporal change of x-ray energies. When radiative recombination processes play a dominant role in emissions, the energy of x rays can be written as follows:

$$I=\sum_{90-100\ \text{Å}\ \alpha,k}\int \Delta E_k R_{d,\alpha}(k) n_t f_{\alpha,k}\,dV = \sum_{90-110\ \text{Å}\ \alpha,k}\int \Delta E_k n_e R_{r,\alpha}(k) n_t f_{\alpha+1,g}\,dV\ , \tag{1}$$

where ΔE_k, $R_{d,\alpha}(k)$, $R_{r,\alpha}(k)$, n_t, $f_{\alpha,k}$, $f_{\alpha+1,g}$, and V denote a transition energy, a radiative lifetime, a radiative recombination rate, a density of total numbers, a normalized population density of an upper level, a normalized population density of a ground state, and a volume, respectively. The subscripts α, k, and g denote ionization stage, excited state, and ground state, respectively. Summation is limited within the wavelength range from 90 to 110 Å. Equation (1) can be reduced to a simplified form using spatially averaged values:

$$I=\sum_{\substack{\alpha,k\\ 90-110\ \text{Å}}} \Delta E_k \bar{R}_{r,\alpha}(k) N_t \bar{f}_{\alpha+1,g} \bar{n}_e\ . \tag{2}$$

Temporal change of the energies for one line $I_{\alpha,k}$ is estimated as follows:

$$\Delta I/I_{\alpha,k}=\Delta\bar{f}_{\alpha+1,g}/\bar{f}_{\alpha+1,g} + \Delta\bar{R}_{r,\alpha}(k)/\bar{R}_{r,\alpha}(k)+\Delta\bar{n}_e/\bar{n}_e\ . \tag{3}$$

From the expression for the radiative recombination rate,[43] the second term in Eq. (2) can be reduced to the temperature change as follows:

$$R_{r,\alpha}(k)=5.2\times10^{-14}(\chi_Z/T_e)^{1/2} \times Z[0.43+0.5\ln(\chi_Z/T_e)+0.47(T_e/\chi_Z)^{1/3}]\ ,$$

$$\Delta\bar{R}_{r,\alpha}(k)/\bar{R}_{r,\alpha}(k)\cong\tfrac{1}{2}(\Delta\bar{T}_e/\bar{T}_e)\ .$$

We discuss effects of changes of (i) electron temperatures and densities and (ii) populations on atomic-number dependence of x-ray decays.

1. *Electron temperatures T_e and densities n_e*

At first, we show that the atomic-number dependence cannot be explained by changes of T_e and n_e if x-ray emissions are considered to occur at the center of the laser focal spot. In this case, we need only the spatial maximum values of n_e and T_e. For simplification, we consider ion temperatures as nearly equal to electron temperatures. Validity of this one-temperature approximation can be satisfied for low temperatures in the case of 4.2×10^{11} W/cm^2 from computational results in the Appendix. At 4.2×10^{12} W/cm^2, computational results also show ion temperatures slightly differ from electron temperatures. Using this approximation, temperature T and a front velocity dX/dt after the end of the laser pulse can be written from Eqs. (A2) and (A3) in similar fashion which appear in Ref. 44 for the one-dimensional spherical expansion case.

$$T=T_\eta(X_\eta/X)^2 \tag{4}$$

$$(dX/dt)^2=(dx/dt)_\eta^2+2(Z+1)/MN_tkT_\eta[1-(X_\eta/X)^2] , \tag{5}$$

where M is the total mass and N_t is the total particle number. The subscript η indicates the values at the end of laser pulse (η). From Eq. (5) the final front velocity $(dX/dt)_\infty$ is obtained as follows:

$$(dX/dt)_\infty^2=(dX/dt)_\eta^2+2(Z+1)/MN_tkT . \tag{6}$$

For picosecond-laser plasmas, since at the end of the laser pulse plasmas do not fully expand, then the first term in Eq. (6) can be safely neglected. Therefore,

$$\begin{aligned}(dX/dt)^2&=2(Z+1)/MN_tkT_\eta[1-(X_\eta/X)^2]\\&=(dX/dt)_\infty^2[1-(X_\eta/X)^2] .\end{aligned}$$

But $(dX/dt)_\infty$ is proportional to an experimentally obtained front velocity. As shown in Fig. 4, this velocity has weak dependence on the atomic number. This sounds reasonable considering the experimental observation that electron temperatures obtained from the x-ray absorption method are about 500 eV and show weak dependence on atomic number.[45] Then, X,dX/dt and T_η show weak dependence on atomic number. Therefore, we conclude that temperature decay dT/dt depends weakly on the atomic number from Eq. (4).

Electron densities vary as $n_t=n_eXS=$const or $n_t=\frac{2}{3}n_eX^3=$const for one- or three-dimensional expansions, respectively, where S is a cross section of the focal spot. For both cases, the relation $|dn_e/dt|\sim|dX/dt|$ is obtained. Therefore, the tendency of temporal change of electron densities is similar to that of electron temperatures, that is, it shows weak dependence on atomic number

In the above calculations, x rays at about 100 Å are assumed to emit from the center of the focal point. At the center, for instance, aluminum ions ionize to charge states from 10 to 12 in our previous computational results.[45] Experimentally, emission lines from helium and lithium-like ions were observed.[45] During plasma expansions, charge states are frozen[46,47] and it is difficult to believe that these highly ionized ions recombine to become ions with the charge state of 4. We think x-ray emissions at about 100 Å occur in low-temperature regions. If we assume for all targets that maximum temperatures are constant and x rays are emitted at different temperature regions, dependence of velocities and x-ray decays on atomic number might be explained. If this idea is correct, for a Zn target ($Z=30$) emissions occur in the highest temperature regions, but we cannot explain why emission energies are high for this target.

2. *Population densities $f_{\alpha+1,g}$*

An alternative explanation is considered for atomic-number dependence of x-ray energies. In Eq. (3), quantitatively, the decay time τ_d of $f_{\alpha+1,g}$ brought about by radiative recombination processes can be expressed as

$$\tau_d=\left[n_e\sum_k R_{r,\alpha}(k)\right]^{-1} . \tag{7}$$

Through Eqs. (1) and (7), decay times seem correlated with x-ray energies. This thought can explain the experimental fact that at the same atomic number decay times take a minimum value and x-ray energies take a maximum value, as shown in Figs. 4 and 5.

IV. CONCLUSION

Dynamic behavior of x-ray emissions near 100 Å generated from laser plasmas was investigated for various target materials experimentally. Characteristic decay times ranging from several 100 to 800 ps were determined accurately using a picosecond laser as functions of the atomic numbers for the first time. Experimentally a YAG laser with a pulse width of 30 ps and 100 mJ of energy was focused on targets. Spectra of emitted x rays were obtained by a newly developed flat-field spectrometer and spectral components ranging from 90 to 110 Å were time-resolved by a streak camera. Results can be summarized as follows.

(1) Decay times were observed to vary considerably for various targets ranging from several 100 to 800 ps. With increasing atomic number from a low-Z target, Al, to a high-Z target, Pb, decay times are decreased.

(2) X-ray energies were also measured and functional dependence on atomic number was found to be strongly negatively correlated with decay times, that is, at the same atomic number x-ray energies take a maximum value and decay times take a minimum value. One possible explanation is that measured line x rays occur mainly through radiative recombination processes and energies are related to decay times as shown in Eqs. (1) and (7).

APPENDIX

Computer simulations were performed to analyze experimental results of temporal behavior of x-ray energies. Many computational models and results concerning x-ray emission from laser plasmas were reported[43,48–56]. In these works, nanosecond lasers were mainly considered for the purpose of laser fusion. We treat x-ray emission from plasmas produced by a picosecond laser.

1. Model

The computational model described here is improved from our previous ones[12,13] to include plasma heating by absorption of laser pulse energy. Rate equations for ground states ($n_{\alpha,0}$) and excited levels ($n_{\alpha,1}$) are as follows:

$$dn_{\alpha,0}/dt=-n_{\alpha,0}n_e[C_{i,\alpha}(0)+R_{r,\alpha-1}(0)+n_eD_{i,\alpha-1}(0)]+n_{\alpha+1,0}n_e[R_{r,\alpha}(0)+n_eD_{i,\alpha}(0)]+n_{\alpha-1,0}n_eC_{i,\alpha-1}(0)\ .$$

$$dn_{\alpha+1}/dt=n_{\alpha,1}\left[\sum_m-\{n_e(D_{e,\alpha}(m,l)+C_{e,\alpha}(l,m)]+R_{d,\alpha}(l,m)\}-n_eC_{i,\alpha}(l)-A_{i,\alpha}(l)\right]$$

$$+\sum_m\{n_e[C_{e,\alpha}(m,l)+D_{e,\alpha}(l,m)]+R_{d,\alpha}(m,l)\}n_{\alpha,m}+n_e[n_eD_{i,\alpha}(l)+E_{c,\alpha}(l)+R_{r,\alpha}(l)]n_{\alpha+1,0}=0\ , \tag{A1}$$

where $R_{d,\alpha}(l,m)$ is a radiative decay rate, $C_{e,\alpha}(l,m)$ $[D_{e,\alpha}(m,l)]$ is a collisional excitation (deexcitation) rate, $A_{i,\alpha}(l)$ is an autoionization rate, $E_{c,\alpha}(l)$ is an electron capture rate, $R_{r,\alpha}(l)$ is a radiative recombination rate, and $C_{i,\alpha}(l)$ $[D_{i,\alpha}(l)]$ is a collisional ionization (three-body recombination) rate, respectively.

We intend to explain x-ray decays of 800 ps which are longer than the laser pulse width and to estimate temporal changes of the quantities T_e, n_e, and $f_{\alpha+1,g}$. For this purpose, we adopted assumptions for simplification. First, the radiation field is not coupled to population densities. In decays longer than 100 ps, densities are low enough for this assumption to be satisfied. Second, as excited states, only two levels associated with the following transitions are added to those included in our previous model:[12,57]

Al V, $1s^22s^22p^43d$-$1s^22s^22p^5$ (108.5 Å, line 1),

Al VI, $1s^22s^22p^33s$-$1s^22s^22p^4$ (109.5 Å, line 2).

These lines are strong resonance lines observed in the spectra of Fig. 2. To demonstrate observed x-ray decay times are determined by radiative recombination processes, we think only two levels are enough. If decay times are to be estimated correctly, many levels must be included and due to coupling among these levels recombination times become shorter.

The equation of continuity and the hydrodynamic equations lead to the following simplified form[58] assuming that (i) temperatures are spatially uniform, (ii) velocity is written as $v=[dX(t)/dt]x/X(t)$, and (iii) the spatial density profile is expressed as a Gaussian form

$$\rho_m=\rho_0\exp[-x^2/X(t)^2]\ ,$$
$$\rho_0=C_0/X\ , \tag{A2}$$
$$d^2X/dt^2=(ZT_e+T_i)/m_iX\ .$$

From the energy conservation law, the following equation is obtained:

$$(\tfrac{1}{2})d(N_eT_e)/dt+(N_eT_e/X)dX/dt=P_a-(3m_e/m_i)(N_e/\tau)(T_e-T_i)\ ,$$
$$(\tfrac{1}{2})d(N_iT_i)/dt+(N_iT_i/X)dX/dt=(3m_e/m_i)(N_e/\tau)(T_e-T_i)\ ,$$
$$P_a=P_{\rm in}\left[1-\exp(-\int k_{ei}dx)\right]\ , \tag{A3}$$

where ρ_0 is mass density at $Z=0$, C_0 is a numerical constant, N is the total number of particles, τ is spatially-averaged electron-electron collision time, and P_a is absorbed laser energy. Incident laser pulse shape $P_{\rm in}$ is assumed as

$$P_{\rm in}=\begin{cases}P_0\sin(t\pi/\eta), & 0\le t\le\eta\\ 0, & \text{others}\ .\end{cases} \tag{A4}$$

Laser pulse wave form has no significant influence on computational results in our case. From measurements of converted second harmonics (0.53 μm) by KD*P crystal (potassium dideuterium phosphate) by a streak camera, the expression of the above equation is confirmed as approximation by choosing η to about 30 ps.

2. Results

Computational results are shown in Fig. 6, by solving the set of coupled equations (A1)—(A4). Curves 1 and 2 denote lines 1 and 2, respectively, for 4.2×10^{11} W/cm^2 of the laser intensity. These two lines are combined into curve 3 at 4.2×10^{13} W/cm^2. Differences between curves 1 or 2 and curve 3 can be explained as follows. Temporal maximum values for electron temperatures $T_{e,\max}$ and average charge number $Z_{\max}$ are 27 eV and 3.7, respectively, for 4.2×10^{11} W/cm^2. At 4.2×10^{13} W/cm^2, ions with charge numbers ranging from 4 to 6 related to line emissions still exist only within 20 ps, and, therefore, after that time ions in the high charge state of 9 become dominant. Differences between curves 1 and 2 are brought about by temporal changes of population densities of ground states with charge numbers of 4 and 5 which feed excited states through recombination processes. But, for a low power density of 4.2×10^{11} W/cm^2, ions related to line emissions are abundant even after the laser pulse is diminished.

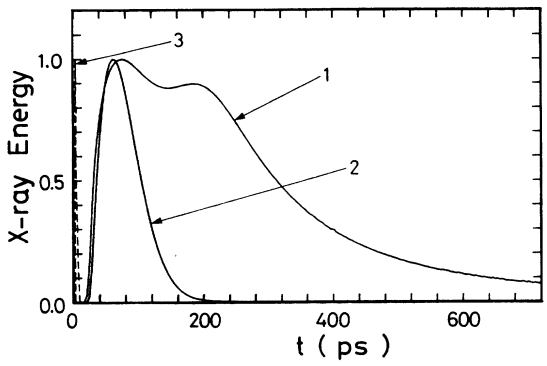

FIG. 6. Computational results obtained by solving the set of coupled equations (1)—(4). The curves 1 and 2 denote line 1 (Al V, $1s^2 2s^2 2p^4 3d$-$1s^2 2s^2 2p^5$, 108.5 Å) and line 2 (Al VI, $1s^2 2s^2 2p^3 3s$-$1s^2 2s^2 2p^4$, 109.5 Å) for 4.2×10^{11} W/cm^2, respectively. These two lines are combined together into the curve 3 in the case of 4.2×10^{13} W/cm^2.

Next, experimental results are compared with computational ones. The experimentally obtained relatively long decay time, 800 ps, can be explained by computational results for 4.2×10^{11} W/cm^2 and is found to be entirely different from results simulated for 4.2×10^{13} W/cm^2. From computational results shown in Fig. 6, terms in the right side of the above equation are evaluated for time ranging from 240 to 720 ps as follows:

$$(1)\ \Delta\bar{f}_{\alpha+1,g}/\bar{f}_{\alpha+1,g}=0.10\ ,$$

$$(2)\Delta\bar{R}_{r,\alpha}/\bar{R}_{r,\alpha}=-0.43\ ,$$

$$(3)\ \Delta\bar{n}_e/\bar{n}_e=0.94\ .$$

Item (1) has the meaning that charge states only change slightly—in other words, are frozen within this time.[46,47] Items (2) and (3) are brought about by plasma expansion. Therefore, decays of x-ray energies are determined mostly by decrease of electron densities and temperatures associated with plasma expansion in this model.

*Present address: New Material Research Center, High Technic Lab., Kawasaki Steel Corp., Kawasaki-cho, Ciba City, Chiba 260, Japan.

[1]A. H. Gabriel and T. M. Paget, J. Phys. B **5**, 673 (1972).

[2]A. H. Gabriel, Mon. Not. R. Astron. Soc. **160**, 99 (1972).

[3]C. R. Bhalla, A. H. Gabriel, and L. P. Prenyakov, Mon. Not. R. Astron. Soc. **172**, 359 (1975).

[4]E. V. Aglitskii, V. A. Boiko, A. V. Vinogradov, and E. A. Yukov, Kvant. Elektron. (Moscow) **1**, 579 (1975) [Sov. J. Quantum Electron. **4**, 322 (1974)].

[5]A. V. Vinogradov, I. Yu. Skobelov, and E. A. Yukov, Kvant. Elektron. (Moscow) **2**, 1165 (1975) [Sov. J. Quantum Electron. **5**, 630 (1975)].

[6]E. V. Aglitskii, A. N. Zherikhin, P. G. Kryukov, and S. V. Chekalin, Zh. Eksp. Teor. Fiz. **46**, 1344 (1977) [Sov. Phys.—JETP **46**, 707 (1977)].

[7]I. Yu. Skobelov, A. V. Vinogradov, and E. A. Yukov, Phys. Scr. **18**, 78 (1978).

[8]V. A. Boiko, S. A. Pikuz, and A. Ya. Faenov, J. Phys. B **12**, 1889 (1979).

[9]A. V. Vinogradov, I. Yu. Skobelov, and E. A. Yukov, Usp. Fiz. Nauk **129**, 177 (1979) [Sov. Phys.—Usp. **22**, 771 (1979)].

[10]J. Dubau and S. Volonte, Rep. Prog. Phys. **43**, 199 (1980).

[11]V. A. Boiko, A. Ya. Faenov, S. Ya. Hahalin, S. A. Pikuz, K. A. Shilov, and I. Yu. Skobelev, J. Phys. B **16**, L77 (1983).

[12]N. Nakano and H. Kuroda, Phys. Rev. A **29**, 3447 (1984).

[13]N. Nakano and H. Kuroda, Appl. Phys. Lett. **45**, 130 (1984).

[14]D. L. Matthews, P. L. Hagelstein, M. D. Rosen, M. J. Eckart, N. M. Ceglio, A. U. Hazi, H. Medecki, B. J. MacGowan, J. E. Trebes, B. L. Whitten, E. M. Campbell, C. W. Hatcher, A. M. Hawryluk, R. L. Kauffman, L. D. Pleasance, G. Rambach, J. H. Scofield, G. Stone, and T. A. Weaver, Phys. Rev. Lett. **54**, 110 (1985).

[15]T. B. Lucatorto and T. J. McIlrath, Phys. Rev. Lett. **37**, 428 (1976).

[16]D. J. Nagel, C. M. Brown, M. C. Peckerar, M. L. Ginter, J. A. Robinson, T. J. McIlrath, and P. K. Carroll, Appl. Opt. **23**, 1428 (1984).

[17]S. Maxon, P. Hagelstein, J. Scofield, and Y. Lee, J. Appl. Phys. **59**, 293 (1974).

[18]J. D. Kilkenny, D. J. Bond, A. J. Cole, D. Everett, T. J. Goldsack, J. D. Hares, R. W. Lee, J. Murdoch, S. J. Veats, L. Cooke, M. J. Lamb, C. L. S. Lewis, J. G. Lunney, A. Moore, M. J. Ward, P. G. Evans, M. H. Key, P. T. Rumsby, A. Raven, W. Toner, T. A. Hall, T. Pugatschew, S. M. S. Sim, O. Willi, in *Laser Interaction and Related Plasma Phenomena*, edited by H. J. Schwarz and H. Hora (Plenum, New York, 1977), Vol. 4A, p. 483.

[19]M. H. Key, C. L. S. Lewis, J. G. Lunney, A. Moore, J. M. Ward, and R. K. Thareja, Phys. Rev. Lett. **44**, 1669 (1980).

[20]G. L. Stradling, Ph.D. thesis, University of California, 1982.

[21]R. L. Kauffman, D. L. Mathews, J. D. Kilkenny, and R. W. Lee (unpublished).

[22]E. M. Campbell, C. E. Max, M. D. Rosen, D. W. Phillion, R. E. Turner, K. Estabrook, B. Lasinski, W. L. Kruer, and W. C. Mead, in *Laser Interaction and Related Plasma Phenomena*, edited by H. Hora and G. H. Miley (Plenum, New York, 1984), Vol. 6, p. 555.

[23]G. I. Brukhnevitch, V. K. Chevokin, Yu. S. Kasyanov, V. V. Korobkin, A. A. Malyutin, A. M. Prokhorov, M. C. Richardson, M. Ya. Schelev, and B. M. Stepanov, Phys. Lett. **51A**, 249 (1975).

[24]H. G. Ahlstrom, J. F. Holzrichter, K. R. Manes, E. K. Storm, M. J. Boyle, K. M. Brooks, R. A. Haas, D. W. Phillion, and V. C. Rupert, in *Laser Interaction and Related Plasma Phenomena*, edited by H. J. Schwarz and H. Hora (Plenum, New York, 1977), Vol. 4A and p. 437.

[25]B. Yaakobi, D. Steel, E. Thorsos, A. Hauer, B. Perry, S. Skupsky, J. Geiger, C. M. Lee, S. Letzring, J. Rizzo, T. Mukaiyasky, E. Lazarus, G. Halpern, H. Deckman, J. Delettrez, J. Sources, and R. McCrory, Phys. Rev. A **19**, 1247 (1979).

[26]H. G. Ahlstrom, *Laser Plasma Interaction*, edited by R. Balian and J-C. Adam (North-Holland, Amsterdam, 1982), p. 245.

[27]N. Nakano, H. Kuroda, T. Kita, and T. Harada, Appl. Opt. **23**, 2386 (1984).

[28]M.-C. Artru and W.-U. L. Brillet, J. Opt. Soc. Am. **64**, 1063 (1974).
[29]S. Bashkin and J. A. Stoner, Jr., *Atomic Energy Levels and Grotrian Diagrams 1, Hydrogen I-Phosphorus XV* (North-Holland, Amsterdam, 1975).
[30]B. Edlèn, *Z. Physik* (Verlag von Julius Springer, Berlin, 1936), p. 621.
[31]J. O. Ekberg and L. A. Svensson, Phys. Scr. **12**, 116 (1975).
[32]S. O. Kastner, M. Swartz, A. K. Bhatia, and J. Lapides, J. Opt. Soc. Am. **68**, 1558 (1978).
[33]B. C. Fawcett, At. Data Nucl. Data Tables **16**, 135 (1975).
[34]J. Davis, P. C. Kepple, and M. Blaha, J. Quant. Spectrosc. Radiat. Transfer **16**, 1043 (1976).
[35]K. D. Lawson and N. J. Peacock, J. Phys. B **13**, 3313 (1980).
[36]B. C. Fawcett and R. W. Hayes, J. Opt. Soc. Am. **65**, 623 (1975).
[37]B. Edlèn, Phys. Scr. **17**, 565 (1978).
[38]E. Ya. Kononov, A. N. Ryabtsev, and S. S. Churilov, Phys. Scr. **19**, 328 (1979).
[39]K. Rashid, Phys. Scr. **22**, 114 (1980).
[40]E. Alexander, M. Even-Zohar, B. S. Frankel, and S. Goldsmith, J. Opt. Soc. Am. **61**, 508 (1971).
[41]J.-F. Wyart, M. Klapisch, J.-L. Schwob, and P. Mandelbaum, Phys. Scr. **28**, 381 (1983).
[42]W. L. Wiese, Phys. Scr. **23**, 194 (1981).
[43]D. Duston and J. J. Duderstadt, J. Appl. Phys. **49**, 4388 (1978).
[44]T. P. Hughes, *Plasmas and Laser Light* (Hilger, London, 1975).
[45]N. Nakano and H. Kuroda, Phys. Rev. A **27**, 2168 (1983).
[46]W. Seka, J. L. Schwob, and C. Breton, J. Appl. Phys. **41**, 3440 (1970).
[47]M. Mattioli, Plasma Phys. **13**, 19 (1971).
[48]D. Colombant and G. F. Tonon, J. Appl. Phys. **44**, 3524 (1973).
[49]K. G. Whitney and J. Davis, Appl. Phys. Lett. **24**, 509 (1974).
[50]D. G. Colombant, K. G. Whitney, D. A. Tidman, N. K. Winsor, and J. Davis, Phys. Fluids **18**, 1687 (1976).
[51]D. Salzmann and A. Krumbein, J. Appl. Phys. **49**, 3229 (1978).
[52]H. D. Shay, R. A. Haas, W. L. Kruer, M. J. Boyle, D. W. Philion, V. C. Rupert, H. N. Kornblum, F. Rainer, V. W. Slivinsky, L. N. Koppel, L. Richards, and K. G. Tirsell, Phys. Fluids **21**, 1634 (1978).
[53]J. D. Perez and G. L. Payne, Phys. Rev. A **21**, 968 (1980).
[54]D. Duston and J. Davis, Phys. Rev. A **23**, 2603 (1981).
[55]D. Duston, R. W. Clark, J. Davis, and J. P. Apruzese, Phys. Rev. A **27**, 1441 (1983).
[56]D. Duston, R. W. Clark, and J. Davis, Phys. Rev. A **31**, 3220 (1985).
[57]N. Nakano and H. Kuroda, Phys. Rev. A (to be published).
[58]N. Nakano and T. Sekiguchi, J. Phys. Soc. Jpn. **51**, 4044 (1982).

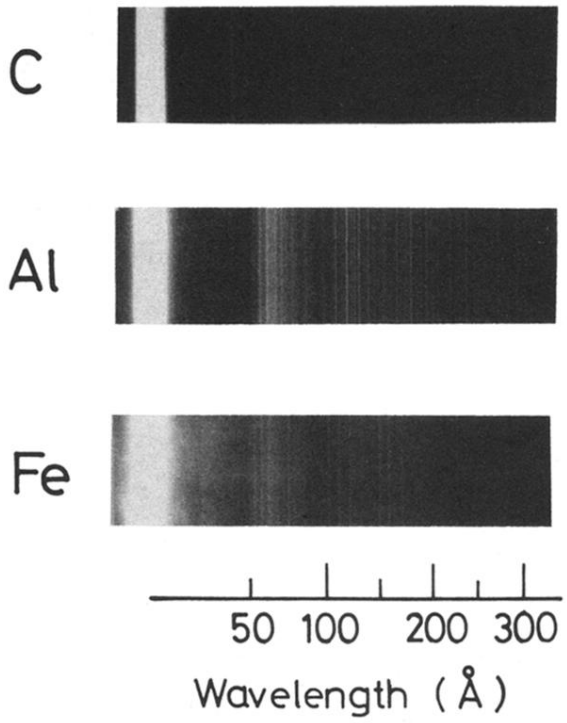

FIG. 2. A typical spectrograph.